DIGITAL ROCKS SIMULATION OF SEISMIC ATTENUATION CAUSED BY WAVE INDUCED FLUID FLOW

Shakil AHMED[1*], **Tobias M. MÜLLER**[1] **and Michael B. CLENNELL**[1]

[1] CSIRO Energy, Kensington, Western Australia 6151, AUSTRALIA
*Corresponding author, E-mail address: shakil.ahmed@csiro.au

ABSTRACT

The aim of this paper is to quantify frictional attenuation associated with local flows induced by seismic waves in a fluid-saturated porous rock. The porous rock matrix is represented by a digitized core sample image. A characteristics of local flow attenuation mechanisms is that the dissipation occurs in the fluid phase due to internal friction. Therefore, it should be possible to quantify wave attenuation by summing up the dissipation in the fluid phase over the course of a wave cycle. This paper is split into two steps. First, pore-scale flow simulations in the laminar flow regime have been performed. The prescribed fluid velocity at the inlet is oscillating, thereby resembling the effect of wave-induced flow. In this approximation the rock matrix is not deforming. A connection with wave attenuation has been made by computing the Rayleigh dissipation function for different frequencies. Second, the workflow has been extended such that solid deformation can be coupled to the fluid motion. Thus, the solutions are two-way coupled. This means that information from the flow field and solid matrix are exchanged through the fluid-structure interface (FSI). To demonstrate this numerical capability a simultaneous flow and deformation simulation for a digitized rock image has been performed.

NOMENCLATURE

$\dot{E}$ Rayleigh dissipation function (W)
E peak strain energy (J)
$\mathbf{F}$ external body force (N)
$\mathbf{I}$ Identity matrix
p hydrostatic pressure (Pa)
Q quality factor (-)
t time (s)
V volume of the fluid phase (m^3)
$\mathbf{v}$ fluid velocity vector (ms^{-1})
δ_{ij} Kronecker delta
$\boldsymbol{\varepsilon}$ fluid strain rate tensor
Φ dissipation due to friction in the fluid phase (W/m^3)
μ, ξ shear and bulk viscosity of the fluid (Pa·s)
ρ density of the fluid (kg/m^3)
$\boldsymbol{\sigma}$ fluid stress tensor (Pa)
ω circular frequency (rads^{-1})

INTRODUCTION

Oscillatory flow of a viscous fluid in deformable porous media induced by seismic waves dissipates some energy as heat and therefore results in seismic wave attenuation and dispersion (Müller et al., 2010). Though this dissipation is typically described through macroscopic equations describing the porous continuum (e.g. Biot, 1962), it has its origin entirely within the fluid phase occupying the pore space of the rock. Therefore simulating fluid flow at the pore scale provides a means to get further insight into the mechanism of wave-induced flow (Müller and Saenger, 2011). Several approaches have been suggested to model attenuation based on digitized rocks. Zhang and Toksöz (2012) combined elastic upscaling simulations with a micro-mechanical model to account for fluid effects and attenuation. Müller and Saenger (2011) used viscoelastic simulations to understand the role of dissipation at the pore scale. Though these approaches yield some insights, in no case is the fluid flow equation solved explicitly. The dissipation within the fluid phase is a well-understood concept (e.g. Pilotti et al., 2002). It has been used to investigate attenuation in digitized rocks (Olson, 1998, 1999). However, the image quality used in these studies is low and the previous results are not conclusive.

Simulations of single phase flow in digitized rock volumes have been performed by various authors (e.g. Olson and Rothman, 1997, Fourar et al., 2004). The focus of these studies is to understand the applicability of Darcy's law for fluid transport through the rock. There is a considerable body of literature on the extraction of the permeability (e.g. Ahmed and Iglauer, 2012, Raeini et al., 2012) from digitized rock simulations. Simulations of two-phase fluid flow using digitized rock models have also been performed (Peszynska and Trykozko, 2013). Schembre-McCabe et al. (2012) give examples of how relevant parameters of the two-phase flow regime can be extracted from digital rocks. Fluid transport is, however, not the main interest of the current paper and therefore will not be reviewed in detail here.

There are several numerical methods available for simulating fluid flow in complex media. Five main approaches can be identified (Maekin and Tartakovsky, 2009): pore network models, lattice gas and lattice Boltzmann methods, Monte Carlo methods, Particle methods (molecular dynamics, dissipative particle dynamics, and smoothed particle hydrodynamics), and grid-based computational fluid dynamics coupled with interface tracking and a contact angle model (e.g. Raeini et al., 2012). An exhaustive review of these methods is beyond the scope of this paper. Our current investigation focuses on numerical aspects of Darcy flow, computing the Rayleigh dissipation function for a rigid rock matrix and we thereby developed a 2 way rock-fluid interaction capability that can be used to quantify the dissipation function and relate this to seismic attenuation. For the case of a rigid rock matrix, we employed an element based finite-volume method for pore spaces by solving the full Navier-Stokes equations. For the deformable rock, we solved full momentum equations (with the finite element method) for the solid matrix.

BASIC EQUATIONS FOR MODELING

Navier-Stokes equations

The aim of this paper is to quantify frictional attenuation associated with local flows induced by waves in a fluid-saturated porous rock. To tackle such a problem at the pore scale numerically means that two sets of equations must be solved in a coupled manner. The mechanical analysis of the solid phase can be based on the equations of dynamic elasticity. Here we refer to Aki and Richards (1980). As the dissipation is exclusively occurring in the fluid phase, we give a short overview of the fluid flow equations in the next section. Specifically we pay attention to how dissipation due to internal friction arises in a Newtonian viscous fluid.

In the presentation of the basic flow equations we follow the terminology of Happel and Brenner (1983). The continuity and momentum equations for a unit volume bound by its control surface are:

$$\frac{\partial \rho}{\partial t} + \nabla \cdot (\rho \, \mathbf{v}) = 0 \qquad (1)$$

$$\frac{\partial (\rho \, \mathbf{v})}{\partial t} + \nabla \cdot (\rho \, \mathbf{vv}) = \nabla \cdot \boldsymbol{\sigma} + \rho \, \mathbf{F} \qquad (2)$$

This is the general form of the Navier-Stokes equation. Here ρ is the fluid density and the fluid velocity vector is $\mathbf{v}$. The fluid stress tensor is $\boldsymbol{\sigma}$. The meaning of the terms of the momentum equation on the left-hand side is as follows. The first term is the rate of increase of momentum per unit volume. The second term is the rate of momentum loss by convection through the control surface, per unit volume. The right-hand side terms have the following meaning. The first term denotes the stresses acting on the surfaces of the unit volume. The second term denotes the external body forces on the element, per unit volume. For a Newtonian fluid the stress tensor is:

$$\boldsymbol{\sigma} = -p\mathbf{I} + \xi(\nabla \cdot \mathbf{v})\mathbf{I} + 2\mu\boldsymbol{\varepsilon} \qquad (3)$$

where p is the hydrostatic pressure. This is the pressure the fluid would be supporting if it were at rest. ξ is the bulk viscosity (related to fluid compressibility), $\boldsymbol{\varepsilon}$ is the strain rate tensor and μ is the shear viscosity (related to transverse transport of momentum). The strain rate tensor is defined as

$$\boldsymbol{\varepsilon} = \frac{1}{2}[\nabla\mathbf{v} + (\nabla\mathbf{v})^*] - \frac{1}{3}\mathbf{I}(\nabla \cdot \mathbf{v}) \qquad (4)$$

where the star symbol means transpose. The stress tensor can be written as

$$\sigma_{ij} = -p\delta_{ij} + \sigma'_{ij} \qquad (5)$$

where the friction tensor is given by

$$\sigma'_{ij} = \mu(v_{i,j} + v_{j,i} - \frac{2}{3}\delta_{ij}v_{k,k}) + \xi\delta_{ij}v_{k,k} \qquad (6)$$

Let us now specify the Navier-Stokes equation for incompressible flow. Incompressible flow means that the fluid density remains constant. Therefore the bulk viscosity term in (3) is neglected. From the continuity equation it then follows that

$$\nabla \cdot \mathbf{v} = 0 \qquad (7)$$

holds. If one further assumes that the shear viscosity is a constant, then the momentum equation specializes to

$$\rho(\frac{\partial \mathbf{v}}{\partial t} + \mathbf{v} \cdot \nabla\mathbf{v}) = -\nabla p + \mu\nabla^2\mathbf{v} + \rho\,\mathbf{F} \qquad (8)$$

This equation corresponds to equation 2-1.15 in Happel and Brenner (1983).

Rayleigh dissipation function

The flux of mechanical energy (a vector field) is the scalar product of local velocity field with the fluid stress tensor,

$$\mathbf{v} \cdot \boldsymbol{\sigma} \qquad (9)$$

The rate per unit time and per unit volume at which energy is supplied by the work done by the stresses on an elementary fluid volume is

$$\nabla \cdot (\mathbf{v} \cdot \boldsymbol{\sigma}) \qquad (10)$$

This power can be represented as (equation 2-2.2 in Happel and Brenner, 1983)

$$\nabla \cdot (\mathbf{v} \cdot \boldsymbol{\sigma}) = -p\nabla \cdot \mathbf{v} + \Phi + \mathbf{v} \cdot (\nabla \cdot \boldsymbol{\sigma}) \qquad (11)$$

The meaning of the terms is as follows. On the left hand side we have the work per unit time and per unit volume done by the stresses acting on an element of fluid volume. It can be decomposed into three parts. The first term on the right hand side is work per unit time done to change the volume of the fluid volume element. The second term is the dissipation term which is work per unit time done on fluid volume element to overcome the internal friction. It is given by

$$\Phi = 2\mu\boldsymbol{\varepsilon}:\boldsymbol{\varepsilon} + \xi(\nabla \cdot \mathbf{v})^2 \qquad (12)$$

The third term is work per unit time done in the motion of the whole fluid volume element. The dissipation integrated over the whole fluid domain is called Rayleigh dissipation function (Happel and Brenner, 1983, equation 2-2.4)

$$\dot{E} = -\int_V \Phi dV \qquad (13)$$

For incompressible flow the dissipation is given by

$$\Phi = 2\mu\boldsymbol{\varepsilon}:\boldsymbol{\varepsilon} \qquad (14)$$

Using (4) this can be further simplified as

$$\Phi = 2\mu[v_{1,1}^2 + v_{2,2}^2 + v_{3,3}^2] +$$
$$\mu[(v_{2,1} + v_{1,2})^2 + (v_{3,2} + v_{2,3})^2 + (v_{1,3} + v_{3,1})^2] \qquad (15)$$

The Rayleigh dissipation function is then

$$\dot{E} = -2\mu\int_V \boldsymbol{\varepsilon}:\boldsymbol{\varepsilon}\, dV$$
$$= -\frac{\mu}{2}\int_V (v_{i,j} + v_{j,i})^2 dV \qquad (16)$$

Here the integration volume extends over the whole fluid domain.

Attenuation due to dissipation and quality factor

In the context of this paper wave attenuation is fully attributed to dissipation in the fluid phase. Therefore, in the general definition of the quality factor (Aki and Richards, 1980) the dissipated energy can be associated with the Rayleigh dissipation function. Thus, we have

$$\frac{1}{Q(\omega)} = \frac{\dot{E}}{\omega E} \qquad (17)$$

where ω is the circular frequency and E is the peak strain energy of a wave cycle. The peak strain energy of the wave cannot be solely computed from flow simulations: the mechanical deformation must be computed too. In other words, to compute an absolute Q value due to wave-induced flow, the coupled problem of flow and solid deformation has to be solved. Note that the peak strain energy is not strongly dependent on frequency. Thus, the frequency dependence of an attenuation mechanism can be studied using the above Q definition if the dissipation $\dot{E}$ is known. This recipe has been used in order to analyse the asymptotic behaviour of attenuation due to wave-induced

2

flow in the presence of mesoscopic heterogeneities (Müller and Rothert, 2006) and will be applied here too.

DIGITIZED RIGID POROUS ROCK SIMULATION

Image processing

This section assumes that the rock is rigid: deformable rock is described in a later section. Numerical simulations of the Navier-Stokes equations for incompressible flow were performed in rock pore spaces obtained from x-ray micro-tomographic images. For deformable rock (explained later), momentum conservation equations were solved for the grains. The pore morphology of the sample was extracted with x-ray micro-tomography (approximately $(5.78\mu m)^3$ voxel size) by segmenting the images based on their greyscale contrast using image processing software. 2D micro-CT image slices were stacked together to generate the 3D F-42 sand pack sample of size 541x431x396 voxels (Figure 1a). A small sub-volume of 100x100x100 voxels was extracted from this sample (Figure 1b) and was used for flow analysis.
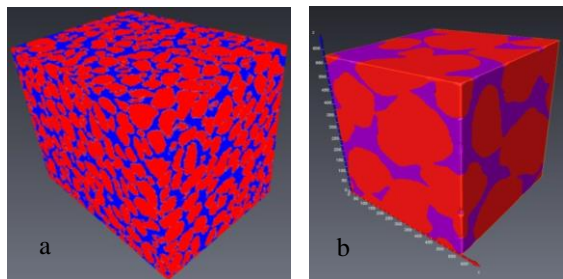
Figure 1: (a) Original sample (541x431x396 voxels) and (b) small sample (100x100x100 voxels) used for flow analysis.

The small sample (100x100x100 voxels) consists of grains and pore spaces. The pore spaces were separated from grains and were used to generate a triangular surface mesh (Figure 2b). The mesh of separated grains (Figure 2a) was used for deformable rock simulation (in a later section). The quality and ability of the triangular surface mesh to generate the tetrahedral volume mesh was checked with orientation, intersection and tetra quality. The surface mesh was then imported into a powerful mesh generating software to generate the volume mesh. Initially the volume mesh of the all pore spaces was generated. For the flow analysis, to save computational expense, all disconnected pore spaces were truncated out of the mesh (Figure 3) as such disconnected void spaces did not contribute to the flow (and in this work only the flow in the connected pore space contributes to attenuation).
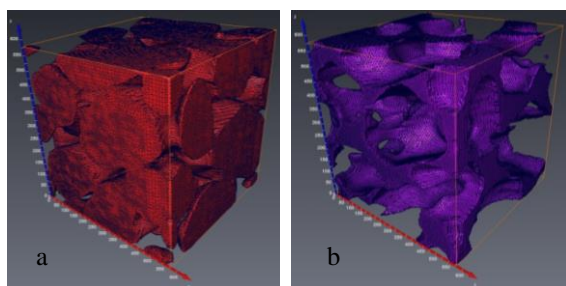

Figure 2: Surface Mesh (a) grains and (b) pore spaces.

Oscillatory Stokes flow

The computations were performed for three-dimensional, transient, isothermal, single phase laminar flow (brine) which simultaneously solves u, v, and w momentum of the Navier-Stokes equation. The software uses an unstructured mesh based on finite volume (FV) method. FV can accommodate any type of grid, so it is suitable for complex geometries. The grid defines only the control volume boundaries and need not be related to a coordinate system.

A uniform sinusoidal brine velocity inlet boundary condition $v_x = (0.0001(\sin(2.0\pi 100 t)))$ was specified. A pressure boundary condition was prescribed at the outlet (opposite side of inlet), and the reference pressure was set to 0. All the other faces were assumed to be impermeable, which was obtained by applying no-slip wall boundary conditions. At the start of the simulation, the sample was fully saturated with brine. Approximately 1.74 million tetrahedral elements were used to generate the volume mesh. A sample volume mesh for the F-42 sand pack is shown in Figure 3. The simulation was run for one complete cycle (0.01s) and the convergence criterion for all variables was set to 10^{-5}.
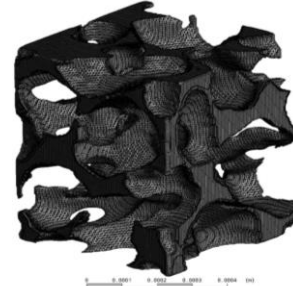

Figure 3: Volume mesh used in flow analysis.

Snapshots of the flow field

All results for the flow field characteristics are shown for the positive peak of the sine wave (i.e. at time 0.0025 sec). Figure 4 shows the pressure drop along the main flow direction and its pore-scale variations. Snapshots of the fluid velocity vectors are shown in Figure 5 and contours in Figure 6. Highest fluid velocities are observed at the centres of the pore channels. This is the expected result as the simulation is limited to laminar flow only and a no-slip boundary condition is applied.
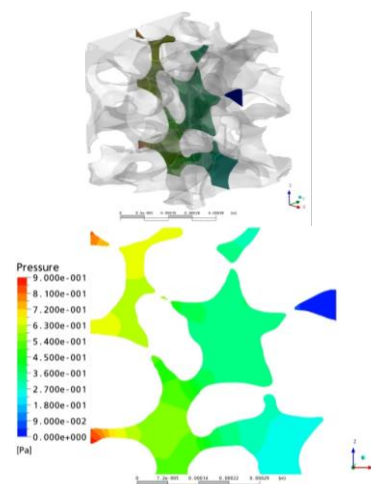

Figure 4: Pressure drop in the mid-plane along the flow direction. The flow is from left to right.

Dissipation function analysis in a rigid porous medium

Figure 7 shows a snapshot of the dissipation per unit volume. In agreement with laminar flow theory, large dissipation is observed in the vicinity of the pore walls. This is due to the existence of viscous boundary layers. The associated viscous skin depth is a function of frequency (not shown here). It is interesting to observe that maximum dissipation occurs close to the pore walls within the narrowest pore channels.
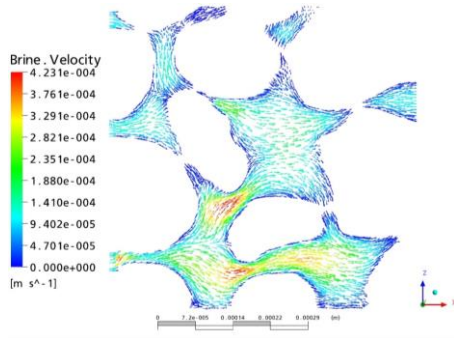

Figure 5: Velocity vector in the mid-plane along the flow direction. The flow is from left to right.
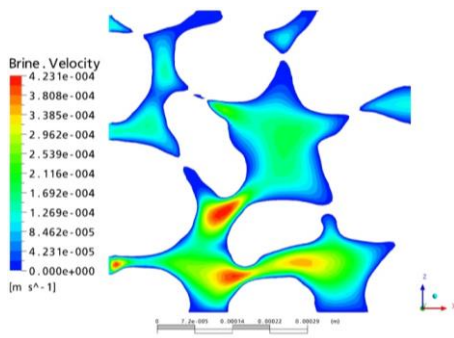
Figure 6: Velocity contour in the mid-plane along the flow direction. The flow is from left to right.
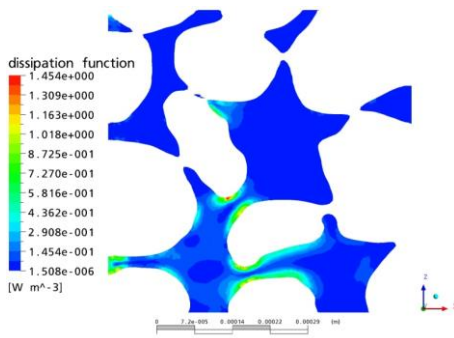

Figure 7: Dissipation function in the mid-plane along the flow direction. The flow is from left to right.

The Rayleigh dissipation function is shown in Figure 8 for different frequencies. As the solid frame in these simulations is rigid, the oscillating fluid flow and the associated dissipation resemble the high-frequency part of the Biot global flow attenuation mechanism (Biot, 1962). Then the peak strain energy, E, in the equation for Q (equation 17) can be assumed to be a frequency-independent constant.
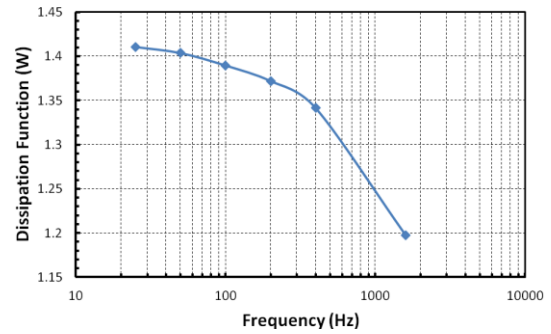

Figure 8: Rayleigh dissipation as a function of frequency. The Biot critical frequency is approximately 750 Hz.

Figure 9 shows the inverse quality factor versus frequency (red symbols) derived from the dissipation function (Figure 8). The blue line corresponds to the high frequency attenuation asymptote $1/\sqrt{f}$ of the Biot global flow attenuation. Therefore, we conclude that the simulation correctly reproduces the expected theoretical behaviour.
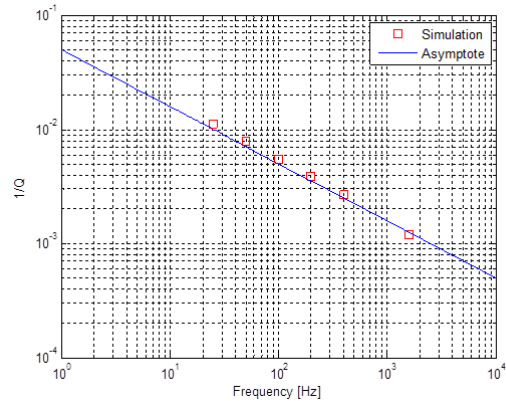

Figure 9: Inverse quality factor versus frequency derived from the dissipation function

DIGITIZED DEFORMABLE ROCK SIMULATION

Numerical modelling procedure

In this section the workflow has been developed such that the solid deformation can be coupled to the fluid motion. For the fluid domain (pore spaces), we obtained three-dimensional transient, incompressible, isothermal, single phase (brine) laminar flow fields by solving the continuity and momentum equations which we described in the previous section. The governing equation for the structural domain (grains) was the momentum conservation equation and was solved on structural elements

The grains were assumed to be elastic, isotropic and homogeneous with a density of 2375 kgm^{-3} and a Young's Modulus and Poisson's ratio of 16 GPa and 0.45 respectively. These values are assumed as a test case only to develop the 2-way coupling. The geometries are shown in Figures 10a and 10b. The boundary conditions in 2-D and 3D are shown in Figures 11 and 12 respectively. For the fluid flow a uniform brine velocity (1x10^{-4} ms^{-1}) inlet boundary condition was specified (in the X direction, Figures 11a and 12a). A pressure boundary condition was prescribed at the outlet (opposite side of inlet, Figure 12a, and the reference pressure was set to 0. All the other faces

were assumed to be impermeable, which was obtained by applying no-slip wall boundary conditions. For the structural analysis (grains), a uniform load of 2 MPa was applied on the top face (Y_{max} in Figure 11b) and the bottom face was held fixed (Figure 11b). Only movement in the Y direction was allowed due to applied load (2 MPa). All the other motions of the control volume were restricted.
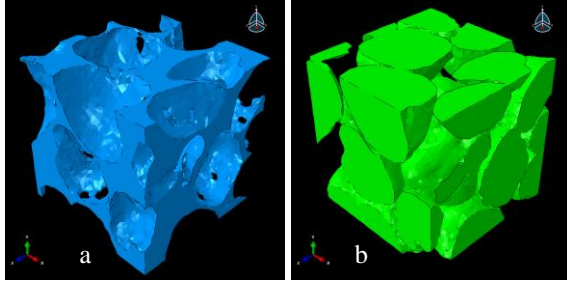

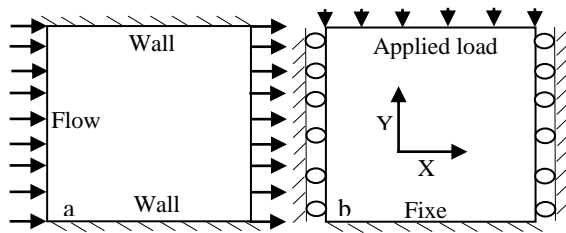**Figure 10:** Geometry of (a) pore spaces and (b) grains.

Figure 11: Boundary conditions (schematic diagram) for (a) the flow and (b) mechanical loading simulations.
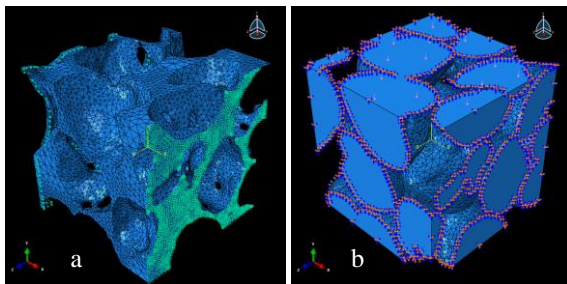

Figure 12: Boundary conditions for (a) pore spaces and (b) grains.

The mesh consisted of tetrahedral elements (Figures 13a and 13b) for both pore spaces and grains. The total number of elements for the pore spaces and grains were 152,890 and 353,192 respectively.
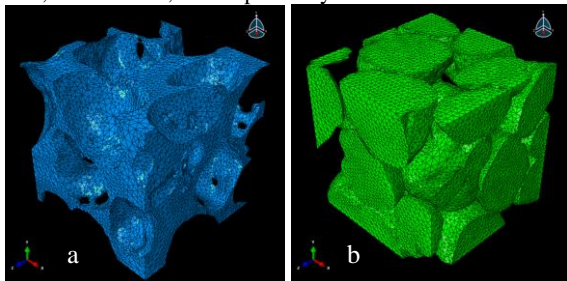

Figure 13: Mesh of (a) pore spaces and (b) grains.

At the start of the simulation, the sample was fully saturated with brine. The simulation was run for 0.2 sec and the convergence criterion for all fluid variables was set to 10^{-5}. The brine in the pore spaces exerts pressure on the grain wall, causing it to deform and, thus, alter the

flow of the fluid. The pressure and shear force from the flow analysis and deformations from the structure analysis were exchanged through a common FSI as shown in Figure 14.
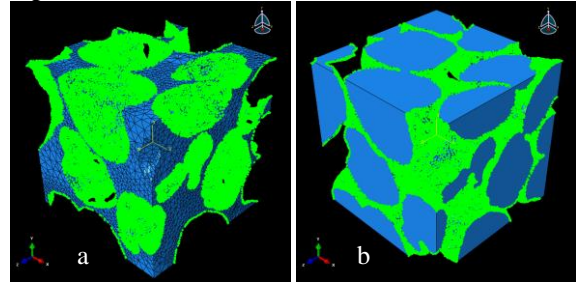

Figure 14: Fluid-structure interface for (a) pore spaces and (b) grains.

Snapshots of coupled deformation and flow fields

All results for the flow field (pore spaces) and structural analyses (grains) are obtained after 0.2 sec. Figure 15b shows the Von-Mises stress induced by the flow field (Figure 15a) and mechanical load (in Y-direction). It is interesting to note that the stress concentrations in the vicinity of grain contacts (Figure 15b) are highest.
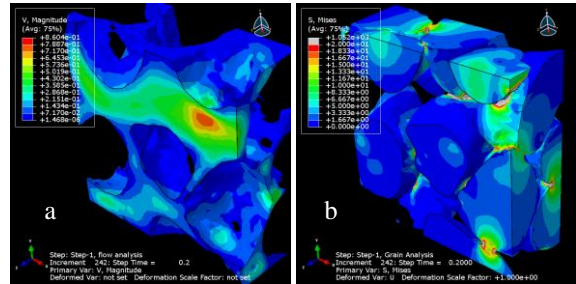

Figure 15: (a) magnitude of fluid velocity in the pore space (b) corresponding Von-Mises stress distribution.

Figure 16a shows the fluid velocity vector field obtained from flow analysis and the displacement field (Figure 16b) obtained from grain analysis. This displacement is the result of both pressure force (solved from flow analysis) and mechanical load (applied as a boundary condition in solid analysis). As the mechanical load is applied at the top of the sample and the bottom is held fixed, the displacement is large at the top and zero at the bottom.
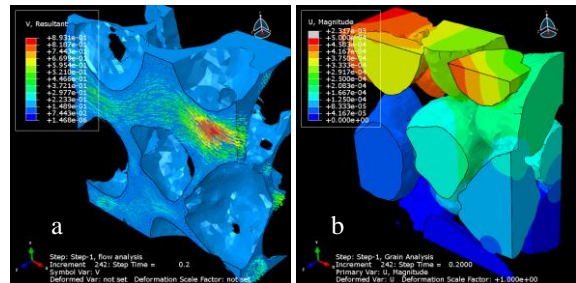

Figure 16: (a) flow velocity vector field and (b) displacement field in the solid part.

The highest fluid velocities are observed at the centre of the pore channels as the simulation is limited to laminar flow only and a no-slip boundary condition is chosen (figures 15a and 16a). The dissipation function for mechanical wave-induced flow can be obtained from the

brine flow field distribution. The details are already explained in the digitized rigid porous rock section.

DISCUSSION

The aim of this paper is to quantify frictional attenuation associated with local flows induced by seismic waves in a fluid-saturated porous rock by numerical means. The paper is split into two steps. First, pore-scale flow simulations in the laminar flow regime in a digitized rigid rock volume are performed. In the next step the workflow is extended such that solid deformation can be coupled to the fluid motion. Our basic assumption here is that wave-induced flow attenuation is associated with local flows driven by induced pressure gradients. These induced pressure gradients are associated with stiffness contrasts and stress concentrations in the solid phase. The local flows are associated with internal friction in the fluid due to a finite fluid shear viscosity. In our current investigation, the solid frame is made of the same material (same stiffness) throughout and there is only a single fluid saturating the pore space. Thus, no significant local pressure gradients can develop. Only very localized stress concentrations are observed in Figure 15b. Moreover, the spatial scales over which these pressure gradients develop govern the characteristic frequency of the fluid pressure relaxation process. Simple analysis shows that the characteristic frequency of attenuation due to wave-induced flow scales as $\omega_c = \dfrac{D}{L^2}$, where D is the diffusivity and L is the characteristic size of the material heterogeneity (Müller et al., 2010). For typical rock/fluid properties it requires L be on the order of centimetres to produce significant attenuation below 100Hz. Or, analogously, in order for squirt flow attenuation to be significant at seismic frequencies, very small crack aspect ratios are needed (Mavko et al., 2009). In other words, for digitized rock images as used in this study with a size of a few grains only and with no small aspect ratio micro-cracks present, it is anticipated that no significant attenuation at seismic frequencies can be predicted using coupled flow-solid deformation simulations. However, by extending the model domain and introducing heterogeneities with a characteristic size of several grains, the developed workflow should be adequate for simulating wave induced attenuation.

REFERENCES

AHMED, S. and IGLAUER, S., (2012), "Brine permeability prediction for sandpacks and sandstones using Navier-Stokes equations and three-dimensional micro-tomography images of pore spaces", *Ninth International Conferences on CFD in the Minerals and Process Industries*, CSIRO, Melbourne, Australia, December 10-12

AKI, K. and RICHARDS, P. G., (2002), "Quantitative Seismology", *Second Edition, University Science Books*, Sausalito, California

BIOT, M.A., (1962), "Mechanics of deformation and acoustic propagation in porous media", *J. Appl. Phys.*, 33, 1482-1498

FOURAR, M., RADILLA, G., LENORMAND, R. and MOYNE, C., (2004), "On the non-linear behavior of a laminar single-phase flow through two and three-dimensional porous media", *Advances in Water Resources*, 27, 669-677

HAPPEL, J. and BRENNER, H., (1983), "Low Reynolds number hydrodynamics", *Kluwer Academic Publishers Group*, The Netherlands

MAVKO, G., MUKERJI, T. and DVORKIN, J., (2009), "The Rock Physics Handbook", *Second Edition, Cambridge University Press*, Cambridge, UK

MEAKIN, P. and TARTAKOVSKY, A.M., (2009), "Modeling and simulation of pore-scale multiphase fluid flow and reactive transport in fractured and porous media", *Reviews of Geophysics*, 47, RG3002

MÜLLER, T.M., GUREVICH, B. and LEBEDEV, M., (2010), "Seismic wave attenuation and dispersion resulting from wave-induced flow in porous rocks - a review", *Geophysics*, 75, 75A147-75A164

MÜLLER, T.M. and ROTHERT, E., (2006), "Seismic attenuation due to wave-induced flow: why Q in random structures scales differently", *Geophysical Research Letters*, 33, L16305

MÜLLER, T.M. and SAENGER, E.H., (2011), "Viscosity scaling of fluid-related wave attenuation mechanisms in porous rocks", *73rd EAGE Conference*, Vienna, Extended Abstract, P304

OLSON, J.F. and ROTHMAN, D.H., (1997), "Two-fluid flow in sedimentary rock: simulation, transport and complexity", *J. Fluid Mech.*, 341, 343-370

OLSON, J.F., (1998), "Toward the simulation of attenuation: oscillatory flow in porous rock", *Earth Resources Laboratory Department of Earth, Atmospheric, and Planetary Sciences*, Massachusetts Institute of Technology, Cambridge, MA 02139

OLSON, J.F., (1999), "Pore-scale simulation of experimentally realizable, oscillatory flow in porous rock", *Earth Resources Laboratory Department of Earth, Atmospheric, and Planetary Sciences*, Massachusetts Institute of Technology, Cambridge, MA 02139

PESZYNSKA, M. and TRYKOZKO, A., (2013), "Pore-to-core simulations of flow with large velocities using continuum models and imaging data", *Computers and Geosciences*, DOI 10.1007/s10596-013-9344-4

PILOTTI, M., SUCCI, S. and MENDUNI, G., (2002), "Energy dissipation and permeability in porous media", *Europhys. Lett.*, 60 (1), 72–78

RAEINI, A.Q., BLUNT, M.J. and BIJELJIC, B., (2012), "Modelling two-phase flow in porous media at the pore scale using the volume-of-fluid method", *Journal of Computational Physics*, 231, 5653–5668

SCHEMBRE-MCCABE, J., SALAZAR-TIO, R. and KAMATH, J., (2012), "Two examples of adding value through digital rock technology", *International Symposium of the Society of Core Analysts*, Aberdeen, Scotland, UK, 27-30 August 2012

ZHANG, Y. and TOSKSÖZ, N.M., (2012), "Computation of dynamic seismic responses to viscous fluid of digitized three-dimensional Berea sandstones with a coupled finite-difference method", *Journal of the Acoustical Society of America*, 132, 630-640